RESEARCH ARTICLE

SUPERCONDUCTIVITY

Revealing hidden spin-momentum locking in a high-temperature cuprate superconductor

Kenneth Gotlieb[1,2]*, Chiu-Yun Lin[2,3]*, Maksym Serbyn[4], Wentao Zhang[2,5], Christopher L. Smallwood[2,3]†, Christopher Jozwiak[6], Hiroshi Eisaki[7], Zahid Hussain[6], Ashvin Vishwanath[8], Alessandra Lanzara[2,3]‡

Cuprate superconductors have long been thought of as having strong electronic correlations but negligible spin-orbit coupling. Using spin- and angle-resolved photoemission spectroscopy, we discovered that one of the most studied cuprate superconductors, Bi2212, has a nontrivial spin texture with a spin-momentum locking that circles the Brillouin zone center and a spin-layer locking that allows states of opposite spin to be localized in different parts of the unit cell. Our findings pose challenges for the vast majority of models of cuprates, such as the Hubbard model and its variants, where spin-orbit interaction has been mostly neglected, and open the intriguing question of how the high-temperature superconducting state emerges in the presence of this nontrivial spin texture.

Many of the exotic properties of quantum materials stem from the strength of spin-orbit coupling or electron-electron correlations. At one end of the spectrum are topological insulators, which have weak electron correlations but strong spin-orbit coupling (*1*, *2*); at the other end are cuprate superconductors, where electron correlations are the dominant interaction. Although unusual forms of spin response in the cuprates have been reported previously (*3*, *4*), the spin-orbit interaction has been mostly neglected or treated as a small perturbation to the Hubbard Hamiltonian and mean field theory in the context of the Dzyaloshinskii-Moriya interaction, leading to negligible changes to the electronic ground state of cuprates (*5*–*9*).

Recently, there has been an upsurge of interest in materials in which both spin-orbit coupling and strong correlations are important because of their potential to induce exotic quantum states (*10*–*13*). In the presence of superconductivity, for example, spin-orbit interaction can have fundamental consequences for the symmetry of the order parameter (*14*), driving unusual pairing mechanisms (*11*, *15*), creating Ising pairs (*16*), and even realizing the conditions for the existence of previously unobserved particles (*17*–*19*).

Spin- and angle-resolved photoemission spectroscopy (SARPES) has been instrumental in studying the consequences of such interplay for the electronic structure of a variety of materials, from heavy fermions to iridates (*20*, *21*), thanks to its ability to simultaneously probe the energy, momentum, and spin structure of quasiparticles. However, because of earlier predictions of negligible spin-orbit interaction in cuprates (*6*), the full spin character of quasiparticles has not been probed experimentally. Here, we report such a study, revealing unexpected consequences of the spin-orbit interaction for the electronic structure of cuprates.

SARPES measurements of overdoped Bi2212

We studied the spin-dependent character of overdoped $Bi_2Sr_2CaCu_2O_{8+\delta}$ (Bi2212) samples (with the superconducting transition temperature T_c = 58 K) with SARPES over a wide range of energies, momenta, temperatures, and photon energies. We performed 10 distinct measurements by coupling our efficient spectrometer (*22*) to a 6-eV pulsed laser source and synchrotron light of different photon energies. The in-plane components of the quasiparticle's spin polarization (P_x, P_y) were mapped as a function of energy and momentum over the entire Brillouin zone, in both the normal and superconducting states [for comparison, see (*23*)]. The spin spectrometer used in this study (*24*) more readily measures in-plane components of spin than the out-of-plane component (P_z). However, as we discuss later, we expect the latter to be negligible and found it to be zero within experimental uncertainty. Figure 1 shows the low-temperature spin-integrated (Fig. 1, B and E) and spin-resolved (Fig. 1, C and F) maps of energy (E – E_F) versus momentum (k) of the quasiparticle spectrum, where E_F is the Fermi energy. Data are shown for two different momentum cuts: along the nodal direction (Γ-Y) (Fig. 1, B and C), where the superconducting gap is zero, and along an off-nodal direction (Fig. 1, E and F), where the superconducting gap is ~10 meV. The location of the cuts (thick black line) and the photoelectron spin components (blue and red arrows) are shown in the insets of Fig. 1, B to F. In Fig. 1 and the rest of the figures, we use blue and red to indicate the two opposite spin components along a given direction, and we hereafter refer to these components as spin-up and spin-down, respectively. The spin polarimeter we used is not subject to the instrumental asymmetries typical of Mott-type detectors that require calibration or renormalization (*24*). The spin polarization measured in this study is therefore intrinsic to the photoelectrons.

Figure 1 summarizes the most surprising findings of this work: the presence of a nonzero spin polarization in Bi2212 and its strong dependence on momentum. Along the nodal direction, we find that the photoelectron spin component perpendicular to Γ-Y is strongly polarized up, as shown by the spin-resolved intensity map in Fig. 1C, which is primarily blue. The corresponding spin polarization P, defined as the relative difference between the numbers of spin-up and spin-down photoelectrons according to $P = (I_\uparrow - I_\downarrow)/(I_\uparrow + I_\downarrow)$, is positive along this entire cut (Fig. 1D). The polarization shows an overall increase as a function of momentum (or energy) from roughly +20% at the Fermi momentum, k_F (Fermi energy, E_F), to as much as +40% for smaller momenta (or higher binding energies), i.e., closer to the Brillouin zone center, Γ.

Notably, when we move away from the nodal direction, the perpendicular photoelectron spin component reverses and is strongly polarized downward, as seen in the spin-resolved intensity map in Fig. 1F, which is primarily red. The reversal of the intensity peak from primarily spin-up to primarily spin-down can be clearly seen in Fig. 1H, where the SARPES spectra at k_F as a function of energy [energy distribution curves (EDCs)] are directly compared for both the nodal and off-nodal cuts.

A closer look reveals a similar increase of the value of spin polarization for the off-nodal cut (Fig. 1G) toward smaller $|k|$ or higher binding energy. In this case, the polarization is negative (P = –15%) at k_F but eventually turns slightly positive (P = +5%) at higher binding energy. In summary, along both of these cuts, we observed an unexpected nonzero spin polarization that

[1]Graduate Group in Applied Science and Technology, University of California, Berkeley, CA 94720, USA. [2]Materials Sciences Division, Lawrence Berkeley National Laboratory, Berkeley, CA 94720, USA. [3]Department of Physics, University of California, Berkeley, CA 94720, USA. [4]Institute of Science and Technology Austria, 3400 Klosterneuburg, Austria. [5]School of Physics and Astronomy, Shanghai Jiao Tong University, Shanghai 200240, China. [6]Advanced Light Source, Lawrence Berkeley National Laboratory, Berkeley, CA 94720, USA. [7]Electronics and Photonics Research Institute, National Institute of Advanced Industrial Science and Technology, Tsukuba, Ibaraki 305-8568, Japan. [8]Department of Physics, Harvard University, Cambridge, MA 02138, USA.
*These authors contributed equally to this work. †Present address: Department of Physics and Astronomy, San José State University, San José, CA 95192, USA.
‡Corresponding author. Email: alanzara@lbl.gov

becomes more positive as one goes toward higher binding energies (i.e., deeper inside the Fermi surface). The observed nonzero spin polarization has been reproduced under different experimental conditions, with different samples and sample surfaces [(Figs. 1 to 4) and (*23*)], different geometry (*25*), and several photon energies. The effect also persists after sample surface exposure to a vacuum of ≈5×10^{-11} torr over several days, the time scale over which some of the experiments described herein were conducted.

Figure 2 shows the evolution of the photoelectron spin polarization along the Fermi surface and at a binding energy of 160 meV (see, e.g., vertical lines in Fig. 1, C and F). The spin-resolved EDCs at k_F and at smaller momenta k_{HBE} (where HBE indicates high binding energy) are shown in Fig. 2, A and B, respectively; the location of each spectrum is shown in Fig. 2C. In both cases, we observe a net spin polarization that decreases away from the node ($\phi = 0°$), eventually reaches zero at an intermediate angle, and for the spectra at $k = k_F$, even switches sign far away from the node. These results are summarized quantitatively Fig. 2D for both $k = k_F$ and $k = k_{HBE}$ [for the full energy dependence of the spin polarization, see (*23*)]. The spin polarization is approximately even about the nodal line, where it reaches its maximum with values as high as +40%. Notably, it is higher at k_{HBE} than at k_F over the entire angular range. On the Fermi surface, the two spin channels $I_\uparrow$ and $I_\downarrow$ are each stronger in different parts of momentum space. By contrast, at higher binding energy (Fig. 2F), the dominant spin channel is spin-up, yielding an overall positive spin polarization.

The presence of any spin polarization in photoemission from Bi2212, let alone a momentum-dependent spin texture, is unexpected. It is therefore imperative, before proceeding to discuss the total spin texture, to assess whether the observed spin polarization is the result of a final state effect or represents physics intrinsic to the spin state of itinerant carriers in the material.

Figure 3 shows the evolution of the spin polarization across the Brillouin zone boundary (M point) (Fig. 3B) and Brillouin zone center (Γ point) (Fig. 3D). Spin-resolved EDCs are shown in Fig. 3B adjacent to the two opposite M points within the first Brillouin zone (points β and γ) and for a point just across the Brillouin zone boundary (α) that is separated by a reciprocal lattice vector from γ. The locations of these measurements are represented by vertical arrows in Fig. 3A. To access this momentum window, we used higher-energy photons: 33 eV. The experimental geometry is shown in fig. S3A, and the measured spin component is perpendicular to the Γ-M direction.

The data show a clear reversal of this component of spin polarization at the two opposite zone boundaries (curves β and γ) and across the zone boundary (curves α and β). The observation of a reversal of the spin polarization at two points very near in emission angle (curves α and β) but on opposite sides of the zone boundary, as well as similar polarizations for points separated by a reciprocal lattice vector and hence having similar momenta (curves α and γ) but nearly opposite emission angles, confirms the intrinsic nature of the effect and its dependence on quasiparticle momentum rather than photoemission angle. Moreover, the presence of a nonzero spin polarization at different photon energies (fig. S3) contributes to the evidence that the observed effect is a property of the quasiparticle initial state rather than being a final state effect.

Final state versus intrinsic effect

We can learn more about the pattern of spin polarization across momentum space by using a well-known property of Bi2212: the presence of an incommensurate superstructure along the *b* axis caused by the modulation of Bi-O layers. This structural distortion creates umklapp bands that are replicas of the main band on the Fermi surface (dotted lines in Fig. 3A), shifted by the superstructure vector along the Γ-Y direction (*26*, *27*). Therefore, the second-order superstructures of the main band, labeled SS1 and SS2, lie near Γ.

These replica bands are clearly visible in the $h\nu = 6$ eV angle-resolved photoemission spectroscopy (ARPES) intensity maps (where h is Planck's constant and ν is frequency) (Fig. 3C) at the two opposite sides of the Γ point and disperse up toward Γ. The spin-resolved EDCs at k_F, measured along the dashed lines in Fig. 3C, are shown in Fig. 3D and measure

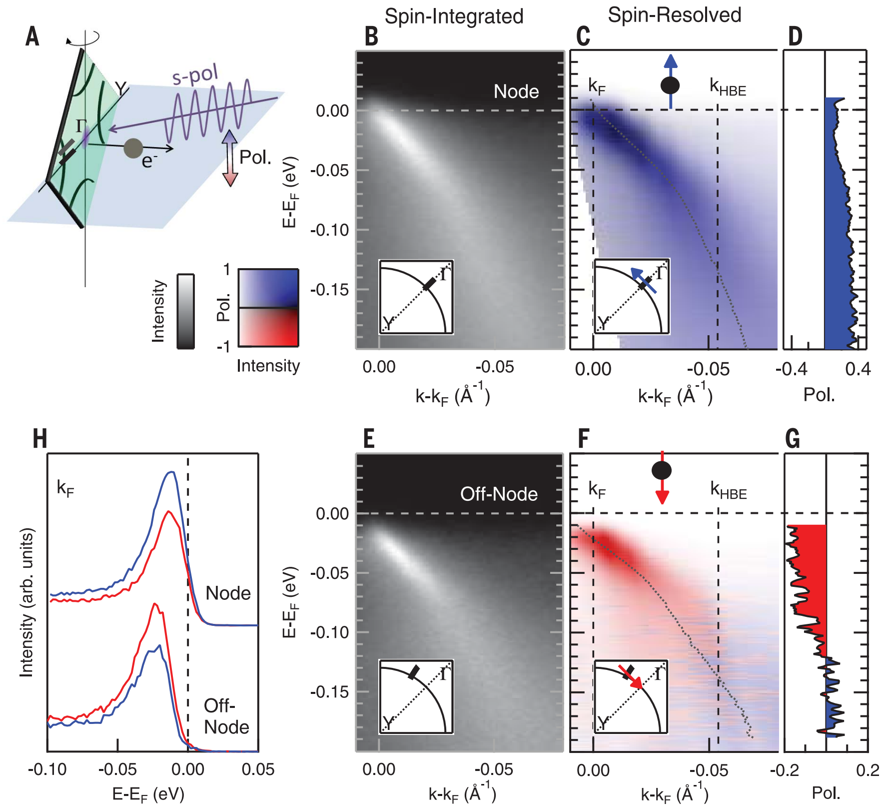

Fig. 1. Spin-resolved measurements along nodal (Γ-Y) and off-nodal cuts. (**A**) Experimental geometry. Pol., polarization; s-pol, s-polarized photons; e⁻, electron. (**B**) Spin-integrated map of the band near E_F along the nodal direction. (**C**) Spin-resolved map taken along the same cut as in (B), with darkness representing photoemission intensity $I_\uparrow + I_\downarrow$ and color representing spin polarization P [see the color scale in (A)]. Momenta k_F and k_{HBE} are the positions of measurements in Fig. 2 where the band is at the Fermi level and high binding energy, respectively. (**D**) Plot of the spin polarization along the band dispersion [dotted gray line in (C)]. (**E** to **G**) Same as (B) to (D) but measured along a cut parallel to the nodal direction that intersects the Fermi surface 14° away from the node, as measured from the zone corner. The same spin component was measured in (B) to (D) and (E) to (G). Insets in (B) to (F) show the location of the cuts (thick black line) and the photoelectron spin components (arrows). In this and subsequent figures, blue and red represent spin-up and spin-down, respectively. (**H**) Spin-resolved EDCs taken at the node, as well as at the Fermi momentum away from the node. arb., arbitrary.

the component of the photoelectron spin perpendicular to the Γ-Y direction. Two clear observations can be made from the data. The first one is that the superstructure bands on the two sides of the Γ point have opposite spin polarization, as seen in the EDCs for SS1 and SS2 in Fig. 3D. This reversal of the spin component through a small angle across the Brillouin zone center (SS1 versus SS2) corroborates the reversal seen at opposite momenta in EDCs β and γ, pointing to a spin polarization that not only is a function of k but also respects time reversal symmetry by switching sign across the Γ point.

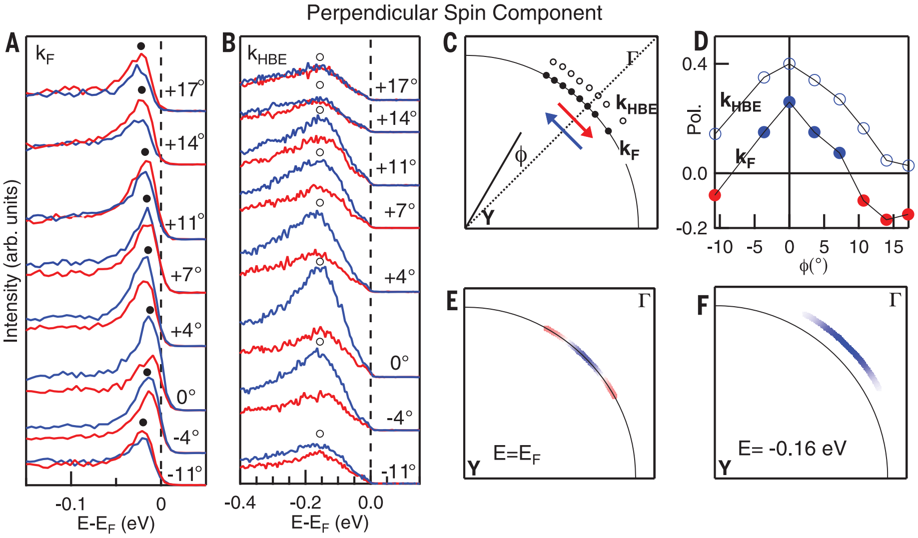

Fig. 2. Spin-resolved measurements along the Fermi surface and at higher binding energy. (**A**) Spin-resolved EDCs taken at momenta along the Fermi surface, as well as (**B**) inside the Fermi surface where the dispersion is at $E_B \approx 160$ meV (where E_B is binding energy). EDCs are marked by φ, the angle from the zone corner (Y point) to k_F, and are taken at momenta indicated in (**C**) one quadrant of the Brillouin zone. The spin component measured was perpendicular to the Γ-Y direction and within the plane of the sample surface. (**D**) Spin polarization as a function of the Fermi surface angle, φ, at k_F (solid circles) and at higher binding energy (hollow circles). (**E** and **F**) Schematics of the texture of this spin component.

The second observation is that at the node, the superstructure bands show opposite spin polarization with respect to the main bands of which they represent a second-order replica. That is, they match the spin of the main band in the same quadrant of momentum space. Though the superstructure band SS2 at $+k$ is the second-order replica of the main band MB2 at $-k$, the spin direction is opposite to that of MB2 (see MB2 in Figs. 3A and 1C for the relative spin polarization). It is the superstructure band SS1 at $-k$ that matches the positive spin polarization of the main band MB2 at $-k$. A more detailed explanation for the opposite value of spin polarization in the replica band relative to that of its "parent band" is found in (*23*); these results provide additional evidence that the observed spin polarization reflects the spin structure of the material bands.

In summary, the dependence of the spin polarization on quasiparticle momentum; the changes in the sign of polarization across the Brillouin zone center and boundaries; the observation of nonzero spin polarizations for different photon energies and geometries with spin alternately parallel and perpendicular to the electric field of light (see Fig. 1 and fig. S3A for more details); and the large values of spin polarization, up to 40%, strongly suggest that the observed effect is intrinsic and cannot be explained solely by an interference between photoemission pathways, as recently proposed (*25*). These findings point to an initial state with a well-defined spin texture in momentum space.

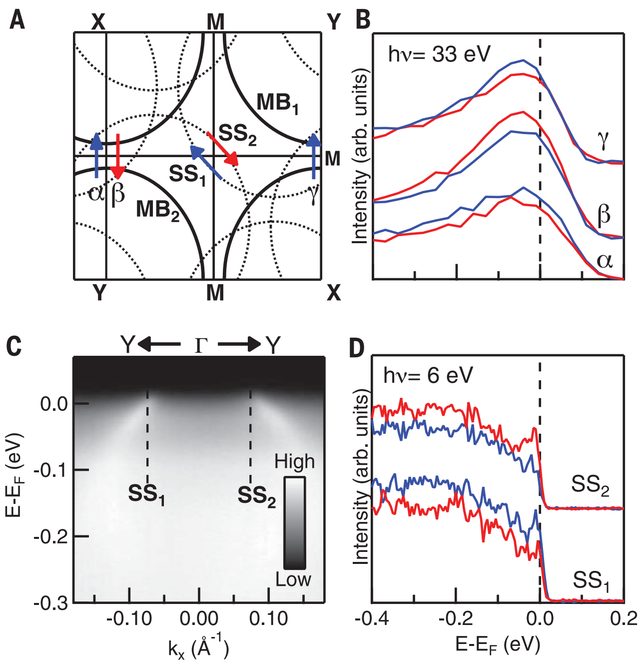

Fig. 3. Measured spin polarization near M points and spin polarization of the superstructures on either side of Γ. (**A**) Spin textures from the two distinct experiments in (**B**) and (**D**) plotted in the Bi2212 Brillouin zone. The main band is shown with thick lines, and its superstructure replicas are shown as thin dotted lines. (B) Spin-resolved EDCs taken with $h\nu$ = 33 eV at momenta shown in (A) near the M points. (**C**) Spin-integrated map of the superstructure taken with $h\nu$ = 6 eV, showing bands that replicate the main band dispersing up as they approach Γ. The dashed lines indicate approximate positions of spin-resolved measurements. (D) Spin-resolved EDCs on either side of Γ.

Full spin texture

Figure 4, A and B, shows the measured momentum-dependent spin polarization parallel to the Γ-Y direction, orthogonal to the spin component presented in Figs. 1 and 2 for several momenta. Spin-resolved EDCs for several momentum cuts are shown in Fig. 4A. For the nodal cut (ε), the intensity peaks are quite similar for the two spin components (Fig. 4A), resulting in nearly zero orthogonal spin polarization (Fig. 4B). At the same time, we see opposite spin polarization at cuts that are displaced by the same angle but in opposite directions from the node (δ and ζ), implying a reversal of the spin polarization component parallel to Γ-Y across the nodal point. Such a reversal is in contrast with the perpendicular spin component (see Fig. 2), which remains the same across the nodal direction.

The full spin texture across the Brillouin zone, obtained from the trends about the nodal line of the parallel and perpendicular spin components, is shown in Fig. 4C. The reversal of the spin polarization across the Γ-Y symmetry line (Fig. 4, A and B) and across the Brillouin zone quadrants (Figs. 2, A and B, and 3D), together with the spin polarization of replica bands, is consistent with a spin texture circling the Brillouin zone center (Γ) clockwise. Meanwhile, at larger k, the larger angle (φ) measurements in Fig. 2B with spin pointing in the direction opposite that at small ϕ indicate that the texture has a more complex momentum dependence. One possibility is a change in the rotation direction of the spin pattern upon approaching boundaries of the Brillouin zone, sketched in gray in Fig. 4C.

The spin-momentum locking inferred in Fig. 4C is reminiscent of a Rashba-type effect. In typical observations of the Rashba effect, however, two bands of opposite spin polarization are split in energy. In this study, we observed only a single spin polarization at any particular momentum, regardless of the band's binding energy at that point. This leads to a single spin texture in k space.

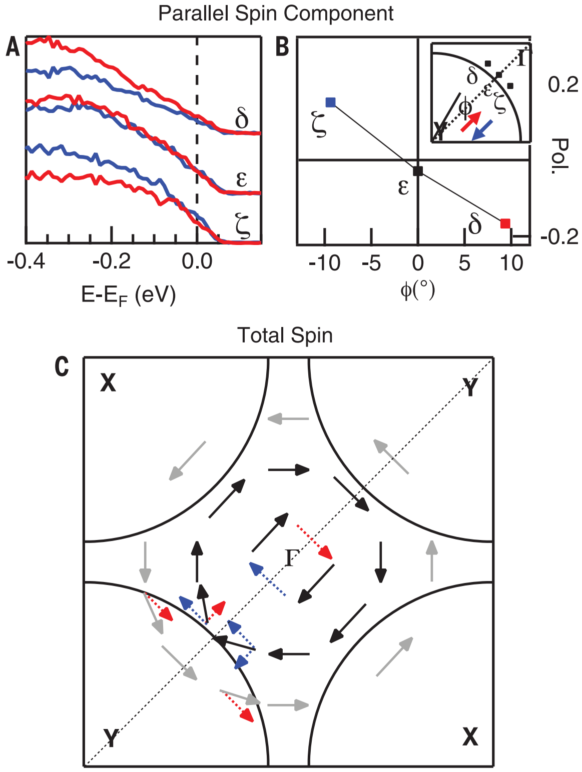

Fig. 4. Total in-plane spin texture. (**A**) Spin-resolved EDCs, acquired with sensitivity to the component of spin parallel to Γ-Y. (**B**) Spin polarization as a function of the Fermi surface angle, ϕ. The inset shows the positions in one quadrant of the Brillouin zone where EDCs were taken. (**C**) Schematic of the addition of the spin textures parallel [from (B)] and perpendicular (from Fig. 2D) to the Γ-Y direction. The counterclockwise circle of gray arrows is consistent with the one component of spin we were able to measure at high k [see (*23*) for further discussion of possible complex spin textures].

Local inversion symmetry breaking

We now present a possible explanation for the observed spin polarization and its momentum dependence and discuss possible implications for superconductivity. Perhaps the most studied spin texture is the Dresselhaus-Rashba effect (*28*, *29*), which is manifested in noncentrosymmetric materials (i.e., materials lacking inversion symmetry) and gives rise to spin-dependent effects, inducing a momentum spin-splitting of the energy bands. Recently, it has been pointed out that even in centrosymmetric materials, a local electric field within the unit cell can lead to spin-split bands (*30*) whereas the net spin polarization remains zero as the electric field averages to zero within the unit cell. This local field can originate from specific structural characteristics that break local inversion symmetry centered on Cu atoms, such as layered structures or some types of lattice distortions that are present in the cuprates (*31*–*36*). In the case of a layered structure, the local field is perpendicular to the planes and the spin-split bands are spatially segregated in real space on top and bottom layers (*30*). In the case of a structural distortion, the spin-split bands are segregated within different parts of the unit cell. The model in (*30*) has been successfully applied to account for the nontrivial spin polarization observed in layered dichalcogenides (*37*, *38*) and a BiS_2-based superconductor (*39*), as well as to explain the nonzero nodal energy splitting between bonding and antibonding bands in a $YBa_2Cu_3O_{6+\delta}$ cuprate superconductor (*9*).

We extend this model to the case of bilayer Bi2212 by using a tight-binding model in the presence of a local electric field, treated via Rashba-type spin-orbit coupling, as in (*30*); the details of the calculations are shown in (*23*). The field is induced by the local breaking of inversion symmetry in Bi2212. Although the crystallographic space group of Bi2212 is often regarded as centrosymmetric (*40*), the local environment of Cu is noncentrosymmetric: The Ca layer separating two Cu-O planes removes the inversion center from Cu. Each Cu-O layer is now subject to a different environment: One Cu-O layer has Bi-O ions above and Ca ions below, whereas this is reversed for the other layer in the unit cell, allowing for a nonzero electric field within the unit cell (see the schematic in Fig. 5A).

Although one would expect both Rashba and Dresselhaus contributions to spin-orbit coupling [R2 and D2 according to the notations in (*30*)], it appears that the dominant components in our experiments come from the Rashba order. This is likely a consequence of the strong anisotropy between *ab* and *c* axes in Bi2212, making the Dresselhaus component subleading. Upon the addition of such spin-orbit coupling, the former bonding (antibonding) band loses its purely antisymmetric (symmetric) character under mirror symmetry. However, we retain this naming convention herein. Both bonding and antibonding bands remain doubly degenerate at any momentum in the Brillouin zone as the crystal retains unbroken inversion and time reversal symmetries. However, these bands acquire spin-momentum locking with opposite spin polarization on each individual Cu-O layer. The spin textures for the antibonding orbital in the two Cu-O layers that result from this model are shown in Fig. 5B. Photoemission measures the interference pattern of contributions from several near-surface layers (*41*) and in this case has different intensity from bonding and antibonding bands (*42*, *43*). Therefore, a nonzero spin signal is expected, despite inversion symmetry and the lack of resolved band splitting. This spin texture stems from differences in photoemission matrix elements for different components of the wave function, as well as the surface sensitivity of the measurement and interference effects. We find that the spin polarization alternates as a function of photon energy, as discussed in (*23*), similarly to the change in the relative strength of photoemission intensity from bonding and antibonding bands (*44*). However, this could also be the result of a more complex dependence of the spin-orbit entanglement on photon energy, as shown extensively in other spin-orbit–coupled materials, such as topological insulators (*41*, *45*), where the sign of spin polarization can change with photon energy and even be zero; more detailed studies and calculations are needed.

By extending our tight-binding model to incorporate interference effects, we remove the perfect cancellation of spin polarizations between bonding and antibonding bands and get a spin texture that reverses sign across the Fermi surface (fig. S6). In addition, the interference effects can also explain the opposite direction of spin polarization between the original bands and their superstructure replicas shown in Fig. 3, as discussed in detail in (*23*).

Although our model can reproduce qualitative aspects of the spin polarization observed in our experiment, it does not capture the magnitude and precise momentum dependence of the spin, which require more involved calculations. Reports in favor of a noncentrosymmetric space group for Bi2212 (*31*, *32*, *46*) might simply argue that it is the absence of any inversion center that allows for the reported nonzero spin texture, as in a standard Rashba system, rather than the creation of a local field. Such a scenario, however, would imply the presence of spin-split bands that have not yet been observed. Moreover, some of the structural

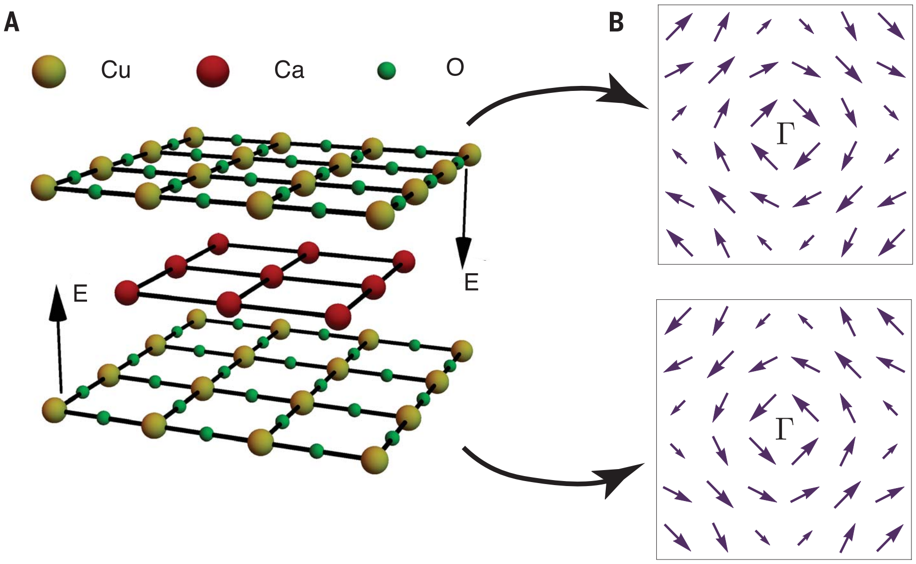

Fig. 5. Spin structure within the unit cell. (**A**) Schematic view of the two-CuO_2 bilayer structure in $Bi_2Sr_2CaCu_2O_{8+\delta}$, where we omit layers of Bi-O and Sr-O which separate bilayers. Green atoms correspond to oxygen, yellow to copper, and red atoms in between are Ca. Arrows schematically depict the possible direction of the electric field, which leads to the spin-orbit coupling of the opposite sign on different layers. (**B**) Expected spin pattern of the antibonding band for two adjacent CuO_2 layers within the unit cell.

distortions typical of cuprates, such as local Jahn-Teller distortions (*32–34*), modulations of the oxygens in the BiO slabs, and buckling of the CuO_2 planes (*47*), could break the local inversion symmetry and give rise to a nonzero electric field. The latter effects along with the presence of other atoms in a polar environment within the unit cell could also potentially contribute to the spin texture reported here and could be responsible for the nonzero spin polarization observed in single-layer Bi2201 (*23*, *25*).

Regardless of the origin of the observed spin-orbit interaction, it is clear that its effect on the symmetry of the Hamiltonian and on the ground state properties cannot be neglected. In the case of weak correlations, the interplay between spin-orbit coupling and superconductivity can affect spin susceptibility (*48*), alter the structure of the gap nodes, and allow for additional Amperean-like attraction channels coming from spin fluctuations (*15*, *49*). In the case of strong correlations, spin-orbit coupling could enhance a charge density wave–type of order (*50*, *51*), as observed in cuprates, and ultimately could affect the superconducting gap and the phase diagram (*52*). Our observation of spin-orbit coupling with a magnitude comparable to that of the interlayer tunneling and superconducting gap [see discussion in (*23*)] and the persistence of a nonzero spin polarization above T_c (fig. S2) suggest that a complex correlation between superconductivity, spin-orbit coupling, and layer degrees of freedom might be at play in cuprates (*52*). As the effects of the coexistence of spin-orbit coupling, strong correlations, and superconductivity are still poorly understood, we hope that our results will stimulate further experimental and theoretical research exploring the physics in this emergent field.

REFERENCES AND NOTES

1. X.-L. Qi, S.-C. Zhang, *Phys. Today* **63**, 33–38 (2010).
2. J. E. Moore, *Nature* **464**, 194–198 (2010).
3. R. E. Walstedt, W. W. Warren Jr., *Science* **248**, 1082–1087 (1990).
4. D. J. Scalapino, *Rev. Mod. Phys.* **84**, 1383–1417 (2012).
5. D. Coffey, T. M. Rice, F. C. Zhang, *Phys. Rev. B* **44**, 10112–10116 (1991).
6. W. Koshibae, Y. Ohta, S. Maekawa, *Phys. Rev. B* **47**, 3391–3400 (1993).
7. V. M. Edelstein, *Phys. Rev. Lett.* **75**, 2004–2007 (1995).
8. C. Wu, J. Zaanen, S.-C. Zhang, *Phys. Rev. Lett.* **95**, 247007 (2005).
9. N. Harrison, B. J. Ramshaw, A. Shekhter, *Sci. Rep.* **5**, 10914 (2015).
10. D. Pesin, L. Balents, *Nat. Phys.* **6**, 376–381 (2010).
11. S. Nakosai, Y. Tanaka, N. Nagaosa, *Phys. Rev. Lett.* **108**, 147003 (2012).
12. W. Witczak-Krempa, G. Chen, Y. B. Kim, L. Balents, *Annu. Rev. Condens. Matter Phys.* **5**, 57–82 (2014).
13. J. G. Rau, E. K.-H. Lee, H.-Y. Kee, *Annu. Rev. Condens. Matter Phys.* **7**, 195–221 (2016).
14. L. P. Gor'kov, E. I. Rashba, *Phys. Rev. Lett.* **87**, 037004 (2001).
15. M. Kargarian, D. K. Efimkin, V. Galitski, *Phys. Rev. Lett.* **117**, 076806 (2016).
16. X. Xi *et al.*, *Nat. Phys.* **12**, 139–143 (2016).
17. L. Fu, C. L. Kane, *Phys. Rev. Lett.* **100**, 096407 (2008).
18. S. Fujimoto, *Phys. Rev. B* **77**, 220501 (2008).
19. J. D. Sau, R. M. Lutchyn, S. Tewari, S. Das Sarma, *Phys. Rev. Lett.* **104**, 040502 (2010).
20. C. Liu *et al.*, *Phys. Rev. B* **90**, 045127 (2014).
21. N. Xu *et al.*, *Nat. Commun.* **5**, 4566 (2014).
22. K. Gotlieb, Z. Hussain, A. Bostwick, A. Lanzara, C. Jozwiak, *Rev. Sci. Instrum.* **84**, 093904 (2013).
23. Materials and methods are available as supplementary materials.
24. C. Jozwiak *et al.*, *Rev. Sci. Instrum.* **81**, 053904 (2010).
25. M. Fanciulli, S. Muff, A. P. Weber, J. H. Dil, *Phys. Rev. B* **95**, 245125 (2017).
26. N. L. Saini *et al.*, *Phys. Rev. Lett.* **79**, 3467–3470 (1997).
27. A. Damascelli, Z. Hussain, Z.-X. Shen, *Rev. Mod. Phys.* **75**, 473–541 (2003).
28. G. Dresselhaus, *Phys. Rev.* **100**, 580–586 (1955).
29. Y. A. Bychkov, E. I. Rashba, *J. Phys. C* **17**, 6039–6045 (1984).
30. X. Zhang, Q. Liu, J.-W. Luo, A. J. Freeman, A. Zunger, *Nat. Phys.* **10**, 387–393 (2014).
31. P. Bordet *et al.*, *Physica C* **156**, 189–192 (1988).
32. V. Petricek, Y. Gao, P. Lee, P. Coppens, *Phys. Rev. B* **42**, 387–392 (1990).
33. X. B. Kan, S. C. Moss, *Acta Crystallogr. B* **48**, 122–134 (1992).
34. A. Bianconi *et al.*, *Phys. Rev. B* **54**, 4310–4314 (1996).
35. B. J. Suh, P. C. Hammel, M. Hücker, B. Büchner, *Phys. Rev. B* **59**, R3952–R3955 (1999).
36. G. M. De Luca *et al.*, *Phys. Rev. B* **82**, 214504 (2010).
37. J. M. Riley *et al.*, *Nat. Phys.* **10**, 835–839 (2014).
38. W. Yao *et al.*, *Nat. Commun.* **8**, 14216 (2017).
39. S.-L. Wu *et al.*, *Nat. Commun.* **8**, 1919 (2017).
40. P. Miles *et al.*, *Physica C* **294**, 275–288 (1998).
41. Z.-H. Zhu *et al.*, *Phys. Rev. Lett.* **110**, 216401 (2013).
42. J. D. Koralek *et al.*, *Phys. Rev. Lett.* **96**, 017005 (2006).
43. T. Yamasaki *et al.*, *Phys. Rev. B* **75**, 140513 (2007).
44. Y. D. Chuang *et al.*, *Phys. Rev. B* **69**, 094515 (2004).
45. Z.-H. Zhu *et al.*, *Phys. Rev. Lett.* **112**, 076802 (2014).
46. A. A. Ivanov *et al.*, *J. Supercond. Nov. Magn.* **31**, 663–670 (2018).
47. M. Opel *et al.*, *Phys. Rev. B* **60**, 9836–9844 (1999).
48. D. Maruyama, M. Sigrist, Y. Yanase, *J. Phys. Soc. Jpn.* **81**, 034702 (2012).
49. P. A. Lee, *Phys. Rev. X* **4**, 031017 (2014).
50. A. Tagliacozzo, E. Tosatti, *J. Phys. C* **12**, L555–L558 (1979).
51. T. Morisaki, H. Wakaura, H. Koizumi, *J. Phys. Soc. Jpn.* **86**, 104710 (2017).
52. C. O. Dias, H. O. Frota, A. Ghosh, *Phys. Status Solidi* **253**, 1824–1829 (2016).

ACKNOWLEDGMENTS

We thank D. H. Lee, C. Varma, E. Altman, and T. L. Miller for fruitful discussion. We thank K. Kurashima for sample preparation. **Funding:** This work was supported primarily by Berkeley Lab's program on Ultrafast Materials Sciences, funded by the U.S. Department of Energy, Office of Science, Office of Basic Energy Sciences, Materials Sciences and Engineering Division, under contract DE-AC02-05CH11231. A.L. acknowledges partial support for this research from the Gordon and Betty Moore Foundation's EPiQS Initiative through grant GBMF4859. The theory component of this paper was supported by the Quantum Materials Program at Lawrence Berkeley National Laboratory, funded by the U.S. Department of Energy, Office of Science, Office of Basic Energy Sciences, Materials Sciences and Engineering Division, under contract DE-AC02-05CH11231. This research used resources of the Advanced Light Source, which is a DOE Office of Science User Facility under contract DE-AC02-05CH11231. M.S. was supported by the Gordon and Betty Moore Foundation's EPiQS Initiative through grant GBMF4307. W.Z. acknowledges support from the Ministry of Science and Technology of China (2016YFA0300501) and from NSF China (11674224). **Author contributions:** K.G. and A.L. were responsible for experimental design. K.G. and C.-Y.L carried out the experiments. Calculations were performed by M.S. and A.V. Samples were prepared by H.E. A.L. was responsible for experiment planning and infrastructure. All authors contributed to the interpretation and writing of the manuscript. **Competing interests:** The authors declare no competing financial interests. **Data and materials availability:** All data are available in the manuscript or the supplementary materials.

SUPPLEMENTARY MATERIALS

www.sciencemag.org/content/362/6420/1271/suppl/DC1
Materials and Methods
Supplementary Text
Figs. S1 to S8
References (*53–58*)
Data S1

13 June 2017; resubmitted 24 February 2018
Accepted 7 November 2018
10.1126/science.aao0980

Science

Revealing hidden spin-momentum locking in a high-temperature cuprate superconductor

Kenneth Gotlieb, Chiu-Yun Lin, Maksym Serbyn, Wentao Zhang, Christopher L. Smallwood, Christopher Jozwiak, Hiroshi Eisaki, Zahid Hussain, Ashvin Vishwanath and Alessandra Lanzara

Science **362** (6420), 1271-1275.
DOI: 10.1126/science.aao0980

Revealing spin-orbit coupling in a cuprate

Strong coupling between the spin and orbital degrees of freedom is crucial in generating the exotic band structure of topological insulators. The combination of spin-orbit coupling with electronic correlations could lead to exotic effects; however, these two types of interactions are rarely found to be strong in the same material. Gotlieb *et al.* used spin- and angle-resolved photoemission spectroscopy to map out the spin texture in the cuprate Bi2212. Surprisingly, they found signatures of spin-momentum locking, not unlike that seen in topological insulators. Thus, in addition to strong electronic correlations, this cuprate also has considerable spin-orbit coupling.

Science, this issue p. 1271